PB89-206676

Video Images of Smoke Dispersion in the Near Wake of a Model Building
Part 1. Temporal an Spatial Scales of Vortex Shedding

(U.S.) Environmental Protection Agency, Research Triangle Park, NC

1988

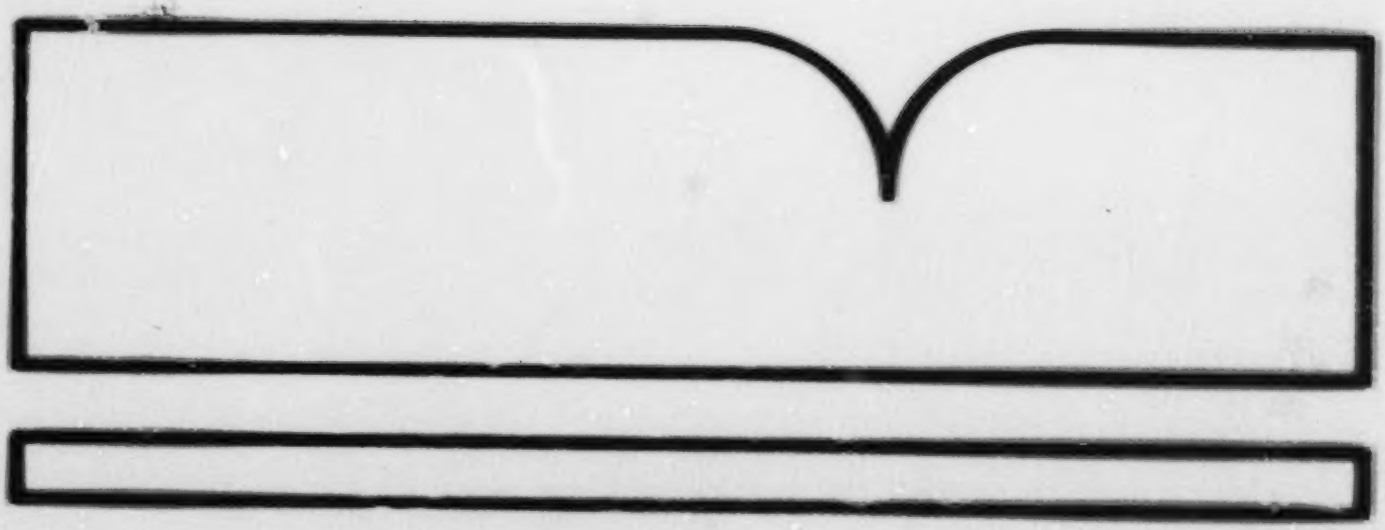

U.S. Department of Commerce
National Technical Information Service

TECHNICAL REPORT DATA (Please read Instructions on the reverse before compl		
1. REPORT NO. EPA/600/J-88/332	2.	3 PB89-206676
4. TITLE AND SUBTITLE VIDEO IMAGES OF SMOKE DISPERSION IN THE NEAR WAKE OF A BUILDING PART I. TEMPORAL AND SPATIAL SCALES OF VORTEX SHEDDING		5. REPORT DATE
		6. PERFORMING ORGANIZATION CODE
7. AUTHOR(S) Alan H. Huber		8. PERFORMING ORGANIZATION REPORT NO.
9. PERFORMING ORGANIZATION NAME AND ADDRESS Same as 12.		10. PROGRAM ELEMENT NO. A101/B/70/09-2056 (FY-87)
		11. CONTRACT/GRANT NO.
12. SPONSORING AGENCY NAME AND ADDRESS Atmospheric Sciences Research Laboratory, RTP,NC Office of Research and Development U. S. Environmental Protection Agency Research Triangle Park, NC 27711		13. TYPE OF REPORT AND PERIOD COVERED
		14. SPONSORING AGENCY CODE EPA/600/09

15. SUPPLEMENTARY NOTES

Journal of Wind Engineering & Industrial Aerodynamics, 31 (1988) 189-223

16. ABSTRACT

In a wind-tunnel study, recorded video images of smoke dispersion in the wake of a rectangular-shaped building were analyzed. A continuous source of smoke was emitted at floor level, midway along the leeward side of the building. Smoke was observed to build up within a region adjacent to the building. Then the smoke was periodically swept away by vortices shed from the leeward building sides and roof. The applicability of analyzing time series of smoke-scattered light for selected quantized video picture elements was favorably demonstrated. Temporal and spatial scales of vortex-shedding of smoke puffs near the center of the wake were quantified through the calculation of spectral densities and autocorrelations. The dominant frequencies (cycles/second) near the center of the wake flow were found to be 0.1-0.3 times the ratio of the velocity to the building height. Estimated integral length scales near the center of the wake flow were found to be 1-2 times the building height.

17. KEY WORDS AND DOCUMENT ANALYSIS		
a. DESCRIPTORS	b. IDENTIFIERS/OPEN ENDED TERMS	c. COSATI Field/Group
18. DISTRIBUTION STATEMENT RELEASE TO PUBLIC	19. SECURITY CLASS (This Report) UNCLASSIFIED	21. NO. OF PAGES 38
	20. SECURITY CLASS (This page) UNCLASSIFIED	22. PRICE MF PC A3, 95 A6.95

EPA Form 2220-1 (Rev. 4-77) PREVIOUS EDITION IS OBSOLETE

EPA/600/J-88/332

Journal of Wind Engineering and Industrial Aerodynamics, 31 (1988) 189–223
Elsevier Science Publishers B.V., Amsterdam — Printed in The Netherlands

VIDEO IMAGES OF SMOKE DISPERSION IN THE NEAR WAKE OF A MODEL BUILDING. PART I. TEMPORAL AND SPATIAL SCALES OF VORTEX SHEDDING

A.H. HUBER*

Atmospheric Research and Exposure Assessment Laboratory, MD-80, U.S. Environmental Protection Agency, Research Triangle Park, NC 27711 (U.S.A.)

(Received August 6, 1987; accepted in modified form January 14, 1988)

Summary

In a wind-tunnel study, recorded video images of smoke dispersion in the wake of a rectangular-shaped building were analyzed. A continuous source of smoke was emitted at floor level, midway along the leeward side of the building. Smoke was observed to build up within a region adjacent to the building. Then the smoke was periodically swept away by vortices shed from the leeward building sides and roof. The recorded signal of the video luminance intensity corresponds to a measurement of smoke-scattered light. The applicability of analyzing time series of video image luminance intensity for selected quantized video picture elements was favorably demonstrated. Temporal and spatial scales of vortex shedding of smoke puffs near the center of the wake were estimated through calculations of spectral densities and autocorrelations. The dominant frequencies (Hz) near the center of the wake flow were found to be 0.1–0.3 times the ratio of the velocity to the building height. Estimated integral length scales near the center of the wake flow were found to be 1–2 times the building height.

1. Introduction

Investigations of dispersion of hazardous air pollution are greatly complicated by the transient nature of atmospheric processes. Traditionally, concentrations of air pollutant and meteorological measurements are sampled at several fixed points over the region and time period of interest (usually 1–24 h). These data in conjuction with available mathematical models are used to infer the overall pattern of pollutant concentration in risk assessments. These limited measurements do not always provide the information necessary to understand adequately all the important processes that affect the dispersion of pollution, especially in situations with significant fluctuations, i.e. near buildings, near mountains, or for chemically reacting pollutants. The temporal and spatial scales that are important to characterize the dispersion of pollution can be better evaluated on the basis of a full picture of the process. Photographs of smoke have been used in research studies to provide a visualization of the

*On assignment from the National Oceanic and Atmospheric Administration, U.S. Department of Commerce.

dispersion patterns both instantaneously and over a time average. Photographs are usually viewed qualitatively because of the time and difficulties involved in quantifying their images.

Exploratory studies at the U.S. Environmental Protection Agency Meteorology Division's Fluid Modeling Facility have demonstrated the applicability of using video images to study the transient flow and dispersion characteristics in the wake of a building (Huber and Arya [1]). The video image format has great potential as an easily quantifiable electronic medium. The application of quantized video picture elements (pixels) in these studies is further demonstrated and evaluated here. Temporal and spatial scales of vortex-shedding using video images of smoke are quantified through spectral density and autocorrelation calculations.

There are numerous wind-tunnel-simulation studies of the visualization and quantification of aerodynamic flows in the wakes of building and hills. A brief overview of some of these studies is presented here to provide some background to this experimental study. There is no unifying theory for characterizing temporal and spatial scales in the wakes from buildings. The aerodynamic wake flow is highly dependent on the particular shape and scale of both the building and the approach boundary layer flow. The simplest view characterizes the near-wake flow as a "cavity" region where recirculation occurs, mean velocities are reduced, and turbulence intensities are increased. The wake flow farther downstream is characterized by a high turbulence intensity and by a mean velocity deficit that progressively decays to background levels. This view provides adequate guidance for pollutant dispersion models used to estimate mean concentrations downstream of the near wake. The basic Gaussian plume model with enhanced dispersion has been shown to provide reasonable estimates for profiles of mean concentrations downwind of buildings, both in wind-tunnel simulations and in full-scale field studies (e.g. Huber and Snyder [2], Huber [3]). This method, however, is not appropriate for estimating concentrations within the wake-cavity region where the build-up of pollutant concentration is associated with increased residence time (e.g. Vincent [4]). Also, estimates of short-term concentrations downwind of the building must include an account of fluctuations due to vortex shedding. The transport of material from the cavity can be dominated by periodic shedding of vortices, particularly for rectangular plates placed normal to the flow (e.g. MacLennan and Vincent [5]).

Hunt et al. [6] provide a complete depiction of the complex flow over and around a building. They have identified several regions of rolled-up shear layers and trailing vortices. Castro [7] and Sakamoto and Arie [8] have measured the shedding frequency within the wakes of rectangular using pulsed-wire and hot-wire anemometry. Both studies have indicated difficulties in detecting a prominent prevailing frequency in flow behind a building that is wider than it is tall. This is believed to be the result of a type of vortex shedding, which may

be changing from the classical von Karman vortex street behind a tall narrow building to an arch-type vortex behind a squat building. MacLennan and Vincent [5] have measured vortex-shedding frequencies by monitoring static pressure just outside the near-wake region. In addition, they have demonstrated how estimates of the shedding frequencies can be related to estimates of cavity residence time.

In the field, variability in atmospheric conditions can considerably complicate an assessment of the aerodynamic building wake flow. It is often difficult to isolate the aerodynamic effects on pollutant dispersion. Because of these problems and the expense involved, wind-tunnel modeling has been used as a more practical method for evaluating building wake influences. Understanding gained from wind-tunnel experimental studies can provide the guidance needed for model development. The experimental studies reported here were planned in this vein. The goal of this research was to develop an understanding of the dispersive processes in the wake of a building in order to include the important aerodynamic effects in a mathematical model of pollutant dispersion in the atmosphere.

This paper demonstrates how analyses of a series of video images can be used to evaluate temporal and spatial scales of the vortex shedding of visual smoke puffs in the wake of a rectangular-shaped model building. The resulting estimates may be rescaled to provide estimates for all sizes of comparably shaped buildings. The building shape and the experimental arrangement were selected to be comparable with those for an earlier study [2]. The shedding frequencies were determined through analyses of spectra; spatial scales of the shed vortices were determined through analyses of autocorrelations. A few point measurements of velocity and hydrocarbon tracer gas were included in this study. Analyses of time series of velocity measurements were compared with those of series of video images. Time-averaged tracer concentrations were compared with those for the video images. Huber and Arya* present analyses of the cross-stream distribution of smoke dispersion in the wake of the building. Part II further evaluated the relationship between the video luminance intensity and tracer concentrations. The video image analyses are shown to be especially applicable to the temporal–spatial distribution, which is very much more difficult to obtain from traditional point tracer measurements.

2. Experimental plan

The experimental study was planned so that there would be cases covering a range of vortex-shedding frequency and dilution of the visualized smoke. The analyses reported here include six cases in which the wake flow behind two

*A.H. Huber and S.P.S. Arya, Video images of smoke dispersion in the near wake of a model building. Part II. Cross-stream distribution, submitted for publication.

different-sized buildings was studied for three different free-stream velocities. Table 1 summarizes the variables that characterize the experimental plan. The building height (H) was 0.1 m for cases 1–3 and 0.2 m for cases 4–6. The along-stream building length was equal to the building height. The cross-stream building length was twice the building height and was oriented perpendicular to the direction of the free-stream flow. The mean velocity upstream of the building at an elevation $z=0.5H$ was used to categorize the flow; it was set at a nominal value $U_n=1$, 2, or 4 m s^{-1}. The study was conducted in the U.S. Environmental Protection Agency's Meteorological Wind Tunnel. The building was placed in a simulated atmospheric boundary layer which is described below. The apparatus and techniques used in these experiments are discussed in the Appendix.

The dispersion of pollution from near buildings should be more rapid at higher flow velocities and slower for larger buildings. The vortex-shedding frequency is expected to be proportional to the ratio U/H. The nominal frequency parameter $F=U_n/H$ ranges from 5 to 40 Hz. Dilution of pollution in the wake of the building is expected to be proportional to H^2U. This dilution results from the vertical and lateral plume spread, each being proportional to the building scale and the along-stream transport, which is proportional to the flow velocity. Here, the nominal dilution parameter $D=H^2U_n$ ranges from 0.01 to 0.16 m^3 s^{-1}. The six planned cases provide an adequate range for evaluating vortex shedding and dilution. Time series for the selected quantized video picture elements of smoke images were analyzed for each of the six cases. Point samples of velocity and hydrocarbon tracer gas were also studied; these data supplement the smoke analyses.

Measurements of the mean velocity and the mean tracer concentration were taken to verify the experimental arrangement. Time series of velocity in the wake of the 0.2-m-high building and in the absence of a building were analyzed for comparison with theory and previous field studies. These results also provide a comparison with the results from image analysis. All the data were taken at a position three times the building height downstream of the leeward building face. This distance is just downstream of the recirculating cavity flow near

TABLE 1

Variables that characterize the experimental plan

Case	H (m)	U_n (m s^{-1})	F (s^{-1})	D (m^3 s^{-1})
1	0.1	1	10	0.01
2	0.1	2	20	0.02
3	0.1	4	40	0.04
4	0.2	1	5	0.04
5	0.2	2	10	0.08
6	0.2	4	20	0.16

the building. It was believed that this position provides the best opportunity to measure the shedding vortices without complications due to significant recirculating flow in the cavity. The source of the smoke and the source of tracer gas were both positioned at floor level, midway along the leeward edge of the building. The origin of the x, y, z coordinate system was set at this same point. Throughout this paper the x- coordinate is downstream, the y- coordinate is cross-stream, and the z- coordinate is the elevation above the floor.

3. Results

3.1. Velocity

Hot-wire anemometry was used to measure mean flow and turbulence in the boundary layer. A cross-wire probe oriented in the x–z plane measured both the along-stream and the vertical components. Vertical profiles of the along-stream mean velocity U and turbulence intensity u'/U (where u' is the standard deviation for u velocity series) in the boundary layer are presented in Fig. 1 for cases having a mean free-stream velocity equal to 4.5 m s^{-1}. The speed in the absence of the building was 3.75 m s^{-1} and 3.3 m s^{-1} at 100 mm and 50 mm respectively; these heights corresponded to $0.5H$ for the 0.2-m-high and 0.1-m-high buildings. Turbulence intensity in the absence of the building was observed to be 20–30% near the surface and to decrease to less than 5% near the top of the boundary layer. The depth of the boundary layer was approximately 1 m. Thus, the two buildings fell within the lower 10–20% of the boundary layer, which is called the surface layer. As expected, the mean speed was reduced and the turbulence intensity was increased in the wake of the building. Their values with the building were observed to be similar to those without the

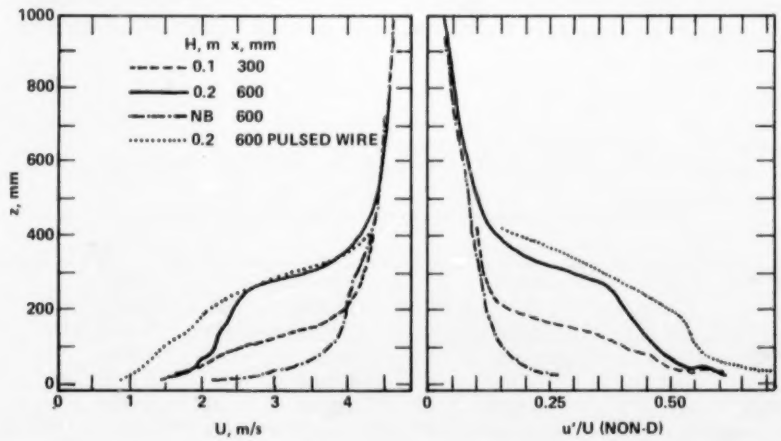

Fig. 1. Vertical profiles of mean velocity and turbulence intensity (NB = no building).

building when measured above 3 times the building height but they deviated substantially below 2 times the building height. The values reported in Fig. 1 were obtained from 2-min averages. A pulsed-wire anemometer was used for supplemental measurements in the wake at $x/H=3$. Pulsed-wire anemometry is necessary for accurate measurement in regions where the turbulence intensity is very high or where flow reversal takes place.

Several 45-s series of 500 velocity samples (cross-wire probe) per second were analyzed so that they could be directly compared with what was done for the smoke pixels (reported in Section 3.3). Table 2 presents a summary for these series taken at $x/H=3, y/H=0, z/H=0.5$. The experimental conditions corresponded to cases 4–6. The point of measurement was at $3H$ downstream of the building at an elevation of $0.5H$. Each measurement was repeated without the building. The along-stream mean velocities in the absence of the building were close (within 10%) of the planned nominal values. The negative mean vertical velocity corresponded to downward motion in the wake of the building. The slight mean vertical velocity in the absence of the building could be caused by upward motion due to the growing boundary layer, or by probe misalignment. Supplemental pulsed-wire series (60 samples per second) were taken to provide measurements in the wake of the building. The along-stream mean velocity in the wake of the building was approximately one-third that in the absence of the building. The standard deviations u' and w' in the wake of the building were respectively 1.5 times and 3.5 times larger than those in the absence of the building.

The pulsed-wire measurements indicated that the cross-wire measurements of the velocity components were substantially in error. The probability densities for the velocity components were studied to help explain these substantial differences. The pulsed-wire probability density functions were symmetric. The u component was negative (indicating flow reversal) about 5% of the time.

TABLE 2

Analysis of six 45-s series of velocity: $x/H=3, y/H=0, z/H=0.5$

Case	H (m)	u (m s^{-1})		w (m s^{-1})	
		U	u'	W	w'
4	0.2	0.48	0.257	−0.00703	0.0981
5	0.2	1.06 (0.71)[a]	0.52 (0.44)[a]	−0.00268 (−0.14)[a]	0.2460 (0.57)[a]
6	0.2	2.07 (1.3)[a]	1.030 (0.80)[a]	−0.00319 (−0.19)[a]	0.4940 (1.0)[a]
4	0.2NB	0.98	0.123	0.0287	0.0659
5	0.2NB	1.96	0.268	0.0856	0.1530
6	0.2NB	3.87	0.553	0.2180	0.2990

Note: NB = no building.
[a]Pulsed wire.

The cross-wire probability densities were symmetric for w, while quite distorted for u. The smaller w' for the cross-wire is very likely due to rectification error when the vertical flow angle is greater than 45° (i.e. the inclination angle of the cross-wires). The distortion for u is greater than can be explained by the small percentage of flow reversal. Apparently, the vertical fluctuations at flow angles greater than 45° contribute substantially to the inflation of u.

Figure 2 presents sample plots of along-stream and vertical velocity fluctuations (u' and w') for case 5. The values for each series were obtained by subtracting the mean and then dividing by the standard deviation. 60 pulsed-wire samples per second are plotted for the series in the wake of the building, while 500 cross-wire samples per second are plotted for the series without the building.

It is believed that these series in the wake of the building are useful for evaluating the dominant frequency and period of correlation. Spectra were calculated for both the cross-wire and the pulsed-wire series. The higher sampling rate that is possible using the cross-wire probe makes it advantageous for avoiding aliasing error. However, only the pulsed-wire probe can provide samples without rectification error. Each spectral density was normalized by the variance for the series. Aside from the aliasing because of the low sampling rate for the pulsed-wire (60 samples per second), the comparison with the cross-wire spectra was excellent. The region affected by aliasing was found to be frequencies higher than the band of dominant low frequencies being evaluated here. The rectification error for the cross-wire does not significantly distort the spectra. Apparently, the rectification error does not affect the frequency distribution of the variance. There are obvious limitations to this finding which need to be further explored. An example of spectra for the cross-wire series is presented below.

Spectra were calculated for the full 45-s series using 500 samples per second for direct comparison with the 45-s series of smoke intensity (reported in Section 3.3). These spectra were not found to deviate significantly from calculation for a 600-s series. The fast Fourier transform within the SAS software package [9] was applied to the series of data. The resulting spectral densities were then smoothed over a bandwidth covering four original values to each side. For example, the smoothed spectra for case 5 are presented in Fig. 3. The plot axes are log-scaled with labeled decades. All plotted frequencies (N Hz) were normalized by the case's nominal frequency parameter (F). Each spectral density $S(N)$ times the frequency was normalized by the variance for the series. These normalized spectra show which frequencies contain the greatest percentage of the variance. For all the series, a high-frequency region was observed to nearly follow a $-2/3$ slope, which corresponds to theoretical estimates and field observation of an inertial subrange (Kaimal et al. [10]).

The dominant normalized frequencies in the absence of the building fell in the ranges 0.02–0.2 and 0.2–2.0 for u and w respectively. For atmospheric boundary layers, spectral frequencies are generally scaled by the elevation of

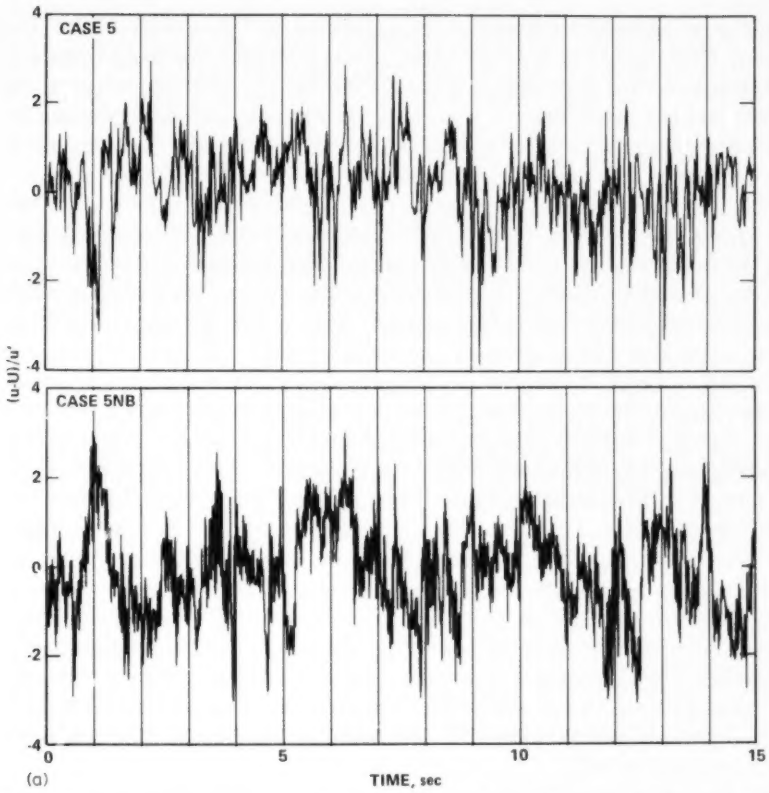

Fig. 2. Fluctuating velocity at $x=600$ mm ($3H$), $y=0$, $z=100$ mm ($0.5H$). (a) Along-stream series.

the measurement. If this were done here, the normalized frequencies would be one half the above-indicated values and the average dominant frequencies would be 0.06 and 0.6 for u and w respectively. Kaimal et al. [10] suggest that comparable near-neutral atmospheric spectra have dominant frequencies at 0.05 and 0.5 for u and w respectively. In practice, most atmospheric spectra have a flat band, which makes the determination of the dominant frequency difficult. The comparison here is quite reasonable and indicates that the frequency distribution of the velocity variance within the simulated atmospheric boundary layer was much like that in the atmosphere.

The spectra in the wake of the building have their dominant frequencies for both u and w in the 0.1–0.3 range, which is much narrower. The similar dominant frequencies for both u and w indicate the influence of shedding vortices. The passage of vortices and the lull in between should impose the same dom-

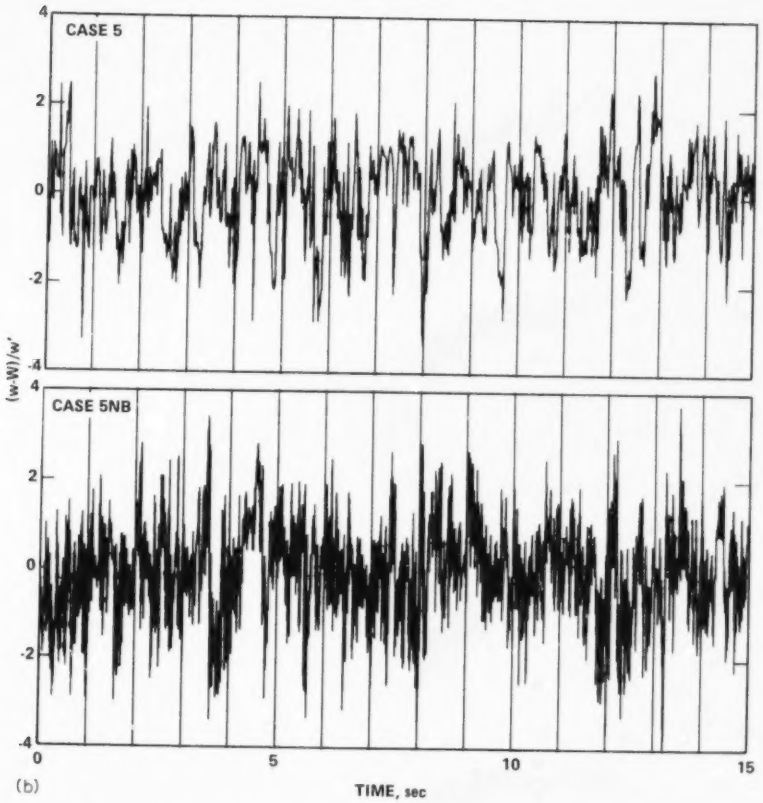

Fig. 2 (cont.). (b) Vertical series.

inant frequency on both u and w. Previous comparable studies [5,7,8] found a prevailing frequency, provided the obstacle was taller than it was wide. As discussed in Section 1, the arch-type vortex associated with a squat building (wider than tall) has less discernible peak frequencies. Most recently, Castro and Haque [11], upon extensively reviewing the literature, have suggested that the shedding frequency should scale with the typical length of the reversed flow region. The reversed flow region, based on a previous smoke study [2], was $2H$ for a building similar to that in this study and the corresponding normalized dominant frequency might be in the range 0.2–0.6, according to the criterion of Castro and Haque.

Autocorrelations for both u and w were also calculated for the full 45-s cross-wire series using 100 samples per second. The autocorrelation program within the SAS software package [9] was used. The results are presented in Fig. 4. A time scale T was defined as the lag time where the correlation was $1/e = 0.368$,

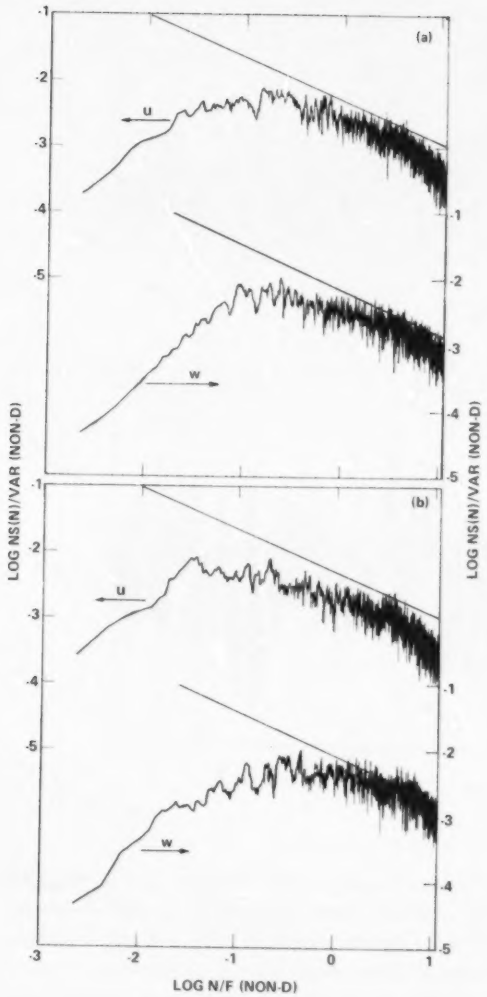

Fig. 3. Spectra for velocity series: (a) case 5, building wake; (b) case 5NB, no building. The solid lines have a $-2/3$ slope.

which is equivalent to the integral time scale, assuming an exponential correlation function $\exp(-\text{lag}/T)$ [12]. This assumption is quite reasonable here. Without the building, temporal scales for u were slightly larger than with the building, and temporal scales for w were 50% smaller than with the building. In the wake of the building, the temporal scale for u was twice that for w.

The product of the integral time scale and the transport speed in the building

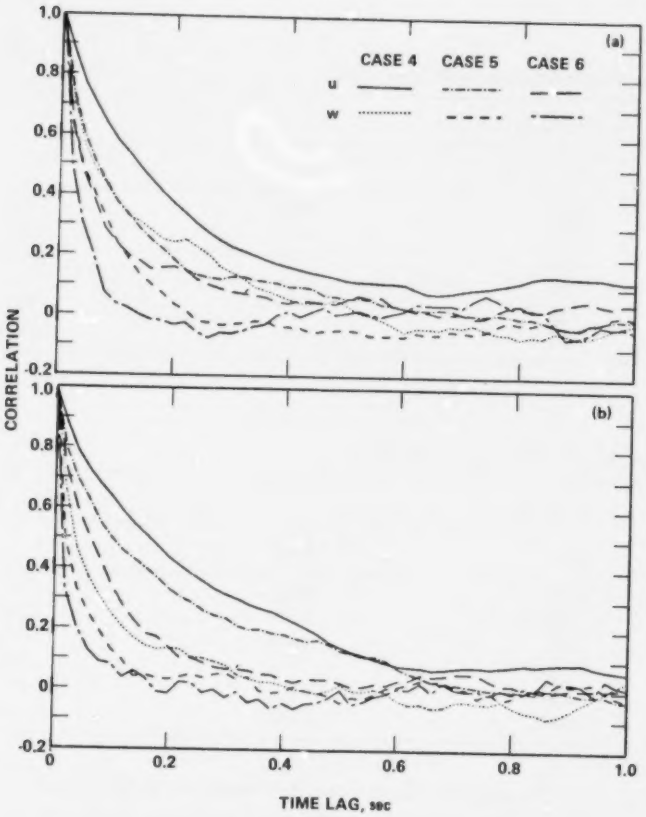

Fig. 4. Autocorrelation for velocity series: (a) all cases, building wake; (b) all cases, no building.

wake should be a reasonable estimate of the characteristic size of the dominant shedding vortices. Spatial correlations are needed to provide the best estimate of a transport velocity. The transport velocity should be reasonably estimated as a value between the mean velocity in the wake of the building and that upstream of the building. This estimate then suggests that the shed vortices might have a streamwise length approximately equal to $0.5H$–$1.0H$.

3.2. Tracer concentrations

Mean concentrations of a hydrocarbon tracer gas were used to evaluate dilution in the wake of the building at $x=3H$. Mean concentrations should be inversely proportional to the building dilution parameter. The values presented in Tables 3 and 4 are 2-min average concentrations. The selected lateral

TABLE 3

Ground-level 2-min-average concentration (ppm) at $x=3H$

Case	Position y/H		
	0	0.5	1
1	3000	2700	2000
2	1700	1600	1400
3	810	730	590
4	740	580	540
5	330	310	250
6	160	150	120

TABLE 4

Centerline 2-min-average concentration (ppm) at $x=3H$

Case	Position z/H		
	0	0.5	1
1	2800	2900	2700
2	1600	1700	1200
3	770	770	490
4	720	750	730
5	350	320	330
6	160	150	150

and vertical positions were the same as those used in the smoke analyses (Section 3.3). This close to the building, the tracer was, over a time average, nearly uniformly mixed. The variation in concentration between cases generally followed the expected variation among the nominal dilution parameters. The concentrations at the uppermost and outermost positions were found to be relatively lower for a few cases. This can be caused by entrainment from above and aside the building. Also, the concentrations this close to the building can be very sensitive to the exact position and the exact size of the cavity region. The changes in concentration were affected by changes in velocity and building scale within 5–15% of the expected. The uncertainty in the tracer analysis is 5–10%.

3.3. Video image analyses

3.3.1. Methodology

Black-and-white video images of smoke were recorded with a camera connected to a standard VHS recorder. The camera was mounted outside the wind

tunnel looking down through a ceiling window (top view) or through a side window (side view). Smoke was produced at the tip of an electrically heated wand. Paraffin oil was forced through a small tube in the center of the wand and vaporized at the hot tip. The vaporized oil was then drawn by and mixed with air through a pipe where the vapor condensed into fine droplets and then emitted into the wind-tunnel flow to simulate a point source emission. The cloud of oil droplets could be more accurately referred to as an oil fog, following Fuks' [13] classification for a condensable aerosol, formed by condensation of super-saturated vapors. He has also summarized a number of other properties of oil fog: aerosols with a liquid phase have particles of true spherical shape even when fused together during coagulation; coagulation within turbulent flow is negligible for very small particles (i.e. particle diameter less than 1μm); particles can be deposited on surfaces. The floor of the tunnel did get wet from deposited smoke. However, most of the smoke appeared to trace the eddy currents of motion and not make contact with the floor. Therefore, it seems reasonable that the number of smoke particles emitted into the building wake will be conserved except for an insignificant fraction that may come into contact with the floor. The preservation of the spherical shape should provide a uniform scattering of light by each particle.

A 600-W floodlight was placed 3 m downstream from the leeward building edge. The light was mounted in the center of the tunnel and elevated approximately 0.3 m. The light was aimed horizontally upstream toward the building. The resulting light, in the absence of the smoke, reflected off the floor, and was observed to be significantly uniform across the areas of interest (the analyzed cross-stream profiles are presented in Part II). The recorded smoke images represent the amount of light reflected and scattered at an approximately 90° angle to the light beam.

The development and application of smoke-scattered light measurement of turbulent concentration fluctuations has been progressing. Rosensweig et al. [14] developed a method for point lighting and point measurement. Lenses and plates with slits were used to collimate and focus a light beam on a point and to focus the scattered light onto a phototube at a 90° angle. This technique was further elaborated by Becker et al. [15]. Shaughnessy and Morton [16] demonstrated the technique for a laser light source. Long et al. [17] expanded the technique to a two-dimensional laser-lighted plane. They used a computer-controlled TV camera to gather intermittently the measurements instantaneously over the entire plane. Most recently, Yip et al. [18] measured time-resolved three-dimensional distributions of concentrations by rapidly sweeping light sheets through the flow volume by rotating mirrors. The above experiments [14–18] were for studies of turbulent jet flow being emitted from a small-scale (e.g. 1 cm) nozzle. There were no problems with setting up all the experimental apparatus around the observed flow. Yang and Meroney [19] developed a laser-light-scattering probe for measuring instantaneous intensi-

ties for smoke puffs in a boundary layer flow. The fiber optics probe allows remote collection of the measurements, which can be quite desirable for some flows. Care had to be taken during the studies reported here to ensure that the experimental apparatus did not cause a disturbance in the flow being studied. 30 video images per second of a full field of view were remotely recorded. Each video image pixel was presumed to represent either a vertically or a laterally integrated profile of particle density. This is different from the previous studies [14–19] that measured point concentrations. The technique reported here could be expanded to give three-dimensional time-resolved measurements by using laser lighting and rotating mirrors.

Van de Hulst [20] provides a supporting theoretical treatise on light scattering. Previous experience represented by the above literature [14–19] has demonstrated the application of smoke-scattered light measurements. The amount of scattered light should be related to the number of particles in the viewed picture element. This is valid for light scattered by either monodispersed or polydispersed particles, provided the overall transmissivity is sufficiently large (i.e. secondary scattering and fluctuations in attenuation noise are insignificant). This condition is believed to be met in this study. However, no special measurements were made to verify this presumption. The evaluation proceeded to demonstrate this new method and initially determine its applicability.

3.3.2. Pixel evaluation

Top- and side-view video recordings of the smoke were taken for each of the six cases. Each recorded picture covered a 1.5 m by 1 m area downstream from the building. Series of video images were viewed repeatedly to develop a conceptual impression of the dispersion and transport processes of the flow in the immediate wake of the building. The smoke built up within a region adjacent to the building and was periodically swept away by vortices shed from the leeward building edges. The shedding appeared to oscillate from one side, then to the other side, and then off the roof. The periodic vortex shedding could be viewed as a peeling off around the building edges. It fits the description of an arch-type vortex in comparison with the more traditional von Karman vortex. All this rapid action was then followed by a lull in action and by smoke buildup. The shed smoke appeared to oscillate from one cross-stream side and then to the other, depending on the timing and strength of the associated vortex. This effect was due in part to the fact that the smoke source was located in the center of what should be a symmetric flow. The oscillations of the observed smoke were not equally distributed for all cases partly because of the sensitivity to the exact building placement. If the smoke source were slightly off the center of the building, the distribution of smoke could be skewed toward one

side. The excess momentum of the smoke exiting from the pipe (pointing downstream) was also observed to affect the distribution. These effects were particularly noticeable for case 1, where the momentum of the pipe-exiting smoke appeared at times to shoot downstream through the center of the wake flow without being flapped to the sides.

Series from each of the six cases were analyzed. A cross-stream strip of the top view at $3H$ downstream of the building was digitized using a video sequence processor (VSP) at North Carolina State University. The VSP digitizes luminance signal from the picture on the basis of a unitless gray scale from 0 to 255. A value of zero would result for zero luminance and a value of 255 would

TABLE 5

Top-view pixel intensity at $x=3H$

Case	Mean	STD	1%	Mean (adjusted)	CV (%)
$y/H=0$					
1	131	28.8	72	59	49
2	160	27.8	90	70	40
3	118	18.9	81	37	51
4	161	27.5	88	73	38
5	190	28.3	121	69	41
6	109	17.3	73	36	48
$y/H=0.5$					
1	89	32.0	49	40	80
1[a]	115	32.0	53	62	53
2	130	41.0	56	74	55
3	118	19.8	77	41	48
4	166	26.1	100	66	40
5	188	27.1	133	55	49
6	104	18.2	66	38	48
$y/H=1$					
1	51	15.3	37	14	109
1[b]	89	32.0	49	40	80
2	81	33.2	44	37	90
3	92	16.7	68	24	70
4	142	35.8	69	73	49
5	168	35.1	93	75	47
6	96	17.0	66	30	57

Note: STD = standard deviation. CV = coefficient of variation.
[a] $y/H=0.25$.
[b] $y/H=0.5$.

TABLE 6

Side-view pixel intensity at $x=3H$

Case	Mean	STD	1%	Mean (adjusted)	CV (%)
$z/H=0$					
1	115	21.3	73	42	51
2	116	21.9	72	44	50
3	103	10.8	84	19	56
4	130	19.9	86	44	45
5	114	17.3	83	31	56
6	99	10.7	80	19	56
$z/H=0.5$					
1	125	28.5	62	63	45
2	123	29.8	61	62	48
3	87	15.5	60	27	57
4	138	28.6	73	65	44
5	109	24.1	61	48	50
6	79	14.8	55	24	62
$z/H=1$					
1	89	37.7	41	48	78
2	109	37.9	47	62	61
3	84	17.5	55	29	60
4	124	36.7	47	77	48
5	110	31.2	47	63	49
6	79	16.7	53	26	64

Note: STD = standard deviation. CV = coefficient of variation.

result for full strength or saturation in the luminance signal. However, the video sequence processor has a guard-band protection which was designed to limit the signal extremes. These limited digitized values fall between 16 and 240. The guard band has been observed to shift on occasions (see discussion in Part II Appendix). The digitized luminance value is referred to here as the video image intensity.

The video image is composed of interlaced rows of picture elements taken at 1/30-s intervals. The odd numbered rows are 1/60 s out of phase with the even-numbered rows. Considering the spatial proximity of adjacent rows of pixels, time series using 60 intensity values per second can be formed. The spectra and correlation analyses reported here were for 45-s series using 60 values per second.

The pixel intensity was presumed to represent an integrated density of smoke particles through the particular field of view; it also included additional lumi-

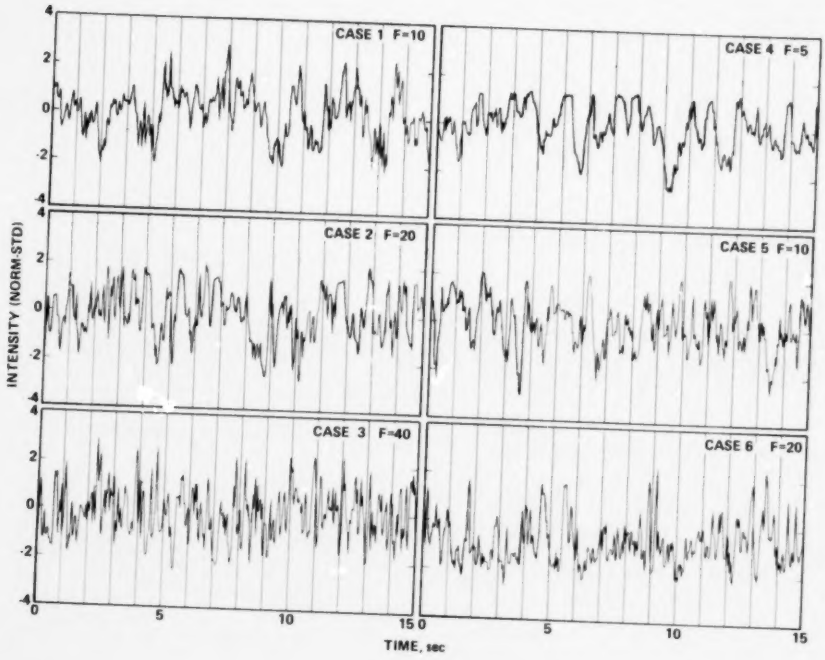

Fig. 5. Fluctuating video image intensity, normalized by the standard deviation from the series mean, for top-view pixels at $x/H=3$, $y/H=0$. The dominant period is inversely proportional to the nominal frequencies F (s^{-1}). The effect of increasing velocity is shown by the vertical column, and the effect of increased building height is seen by comparing across the column.

nance from light scattered and reflected from the surroundings. There were differences throughout each picture in the apparent reflection from the background. Differences among pixel values result from electronic noise from the camera, recorder and digitizer, and from imperfections and vignetting in the camera optics. Factory specifications indicated that the camera response was linear. A check on the camera linearity was performed (see discussion in the Appendix). Linear offsets in mean intensity for these effects should be correctable by pixel-by-pixel adjustments. The mean intensity would be correctable for any nonlinearities in signal recording and processing by using a transfer function. The standard deviation of a series of pixel intensities would not be influenced by linear offsets but would be influenced by nonlinear effects as well as the range of values. The part of the intensity due to smoke can be evaluated by subtracting the intensity in the absence of smoke, provided light

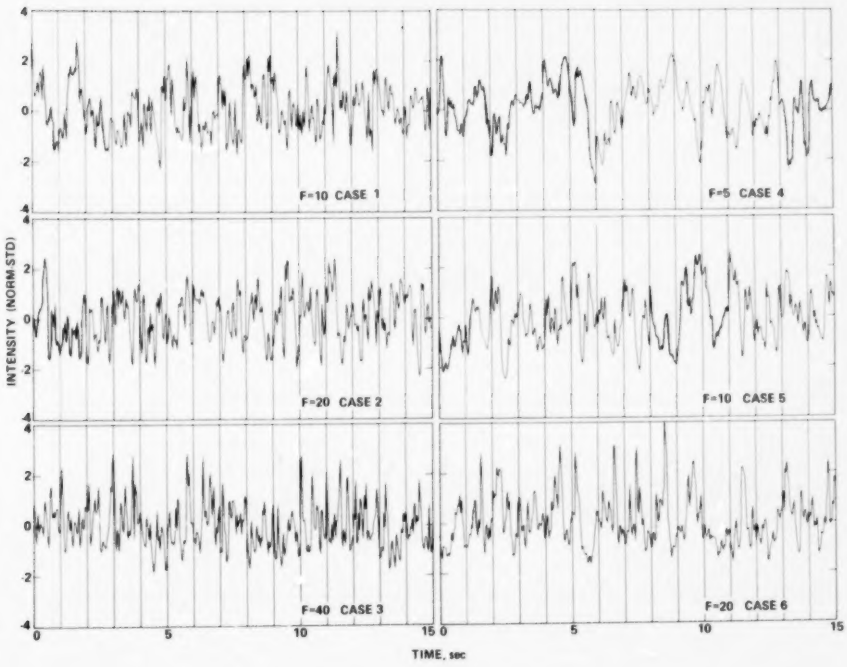

Fig. 6. Fluctuating video image intensity, as in Fig. 5, but for side-view pixels at $x/H=3, z/H=0.5$.

is not reflected from particles to background. Some reflection from the smoke was observed to influence the background level. For this reason analyses of cross-stream distributions were corrected for background by subtracting the lowest values near the tails of the cross-stream distributions (see Part II). Herein, since each sequence of shedding-vortices was observed to contain periods of little smoke, the first percentile value at each pixel was used to adjust for differences in background and other effects. This type of adjustment provides for the best identification of the shedding concentrated puffs.

Tables 5 and 6 present several statistics for the intensities among the six cases. The six cases were for structurally similar situations differing only in the building and velocity scales. Differences in mean intensities at similar positions should be due mostly to differences in the streamwise dilution of the smoke. Streamwise dilution is proportional to the flow velocity. The camera aperture was 1 f-stop smaller for cases 1 and 4 which had a nominal velocity of 1 m s^{-1}. The change in one f-stop should halve the recorded adjusted intensity. This was necessary to avoid saturation of the recorded smoke picture signal. The instantaneous smoke density should be inversely proportional to the velocity, and to building scale even though mean dilution of the tracer was pro-

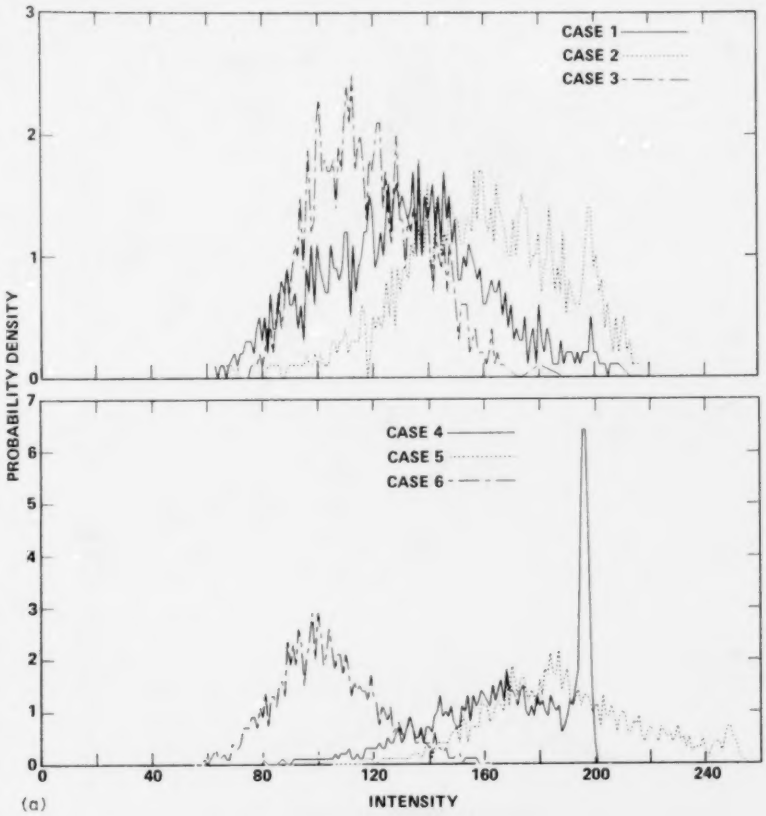

Fig. 7. Distributions for video image intensity series for top-view pixels at $x/H=3$, $y/H=0$: (a) probability density for original values.

portional to H^2U because the image intensity was density of particles integrated through one dimension. Thus, the mean adjusted intensity for case 3 should be roughly half that for cases 1 and 2, and similarly case 6 should be half that for cases 4 and 5; intensities for cases 4, 5 and 6 should be half those for cases1, 2, and 3 respectively.

Case 1 presented a problem in that smoke was spread less in the cross-stream direction because the source jetted somewhat through the cavity flow at low speed near the small building. The revised positions for case 1 more accurately represent the comparable cross-stream position. There is added uncertainty for the very low velocity cases 1 and 4 owing to differenc. s in the wind-tunnel boundary layer flow and building surface flow. Case 5 for the top view was

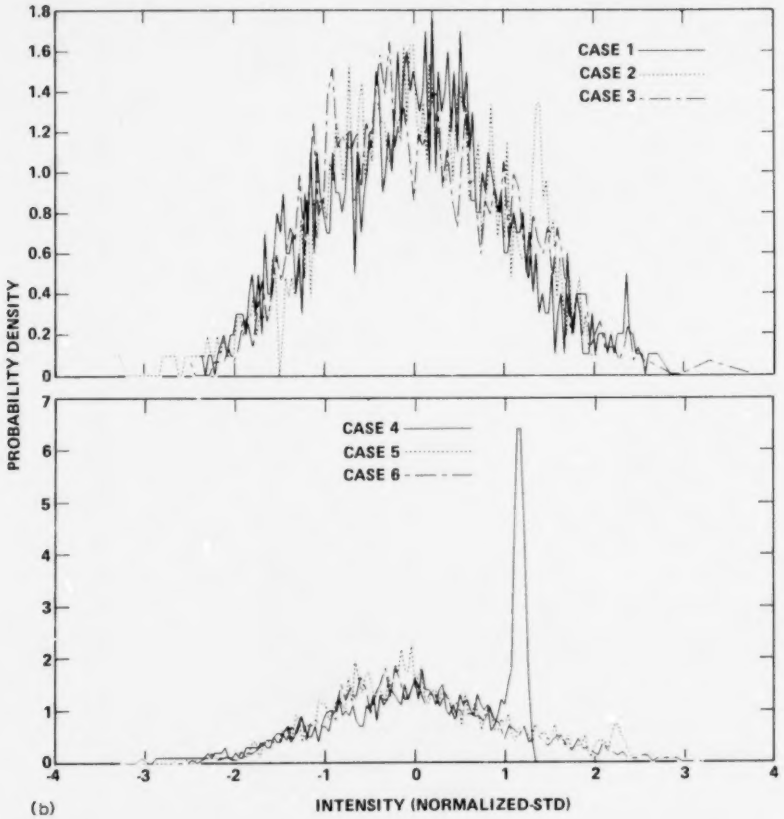

Fig. 7 (cont.). (b) Probability density for normalized values.

processed with the guard band known to be shifted by +15 (see discussion in Part II Appendix). The adjusted mean and standard deviation (STD) followed the expected effect of changing velocity for each building. The values for the 0.2-m building were not half those for the 0.1-m building, as expected. It is reasonable to expect that the difference is due mostly to reduced illuminance (inversely proportional to the square of the distance from the light) and to differences in the light-scattering angle between the light beam and the camera.

There are several other possible reasons to expect some differences among the cases' mean values. The ratio of the building height to the depth of the flow boundary layer will be different between the cases for the two buildings. There could be some effect of light reflection off the building. There could be slight

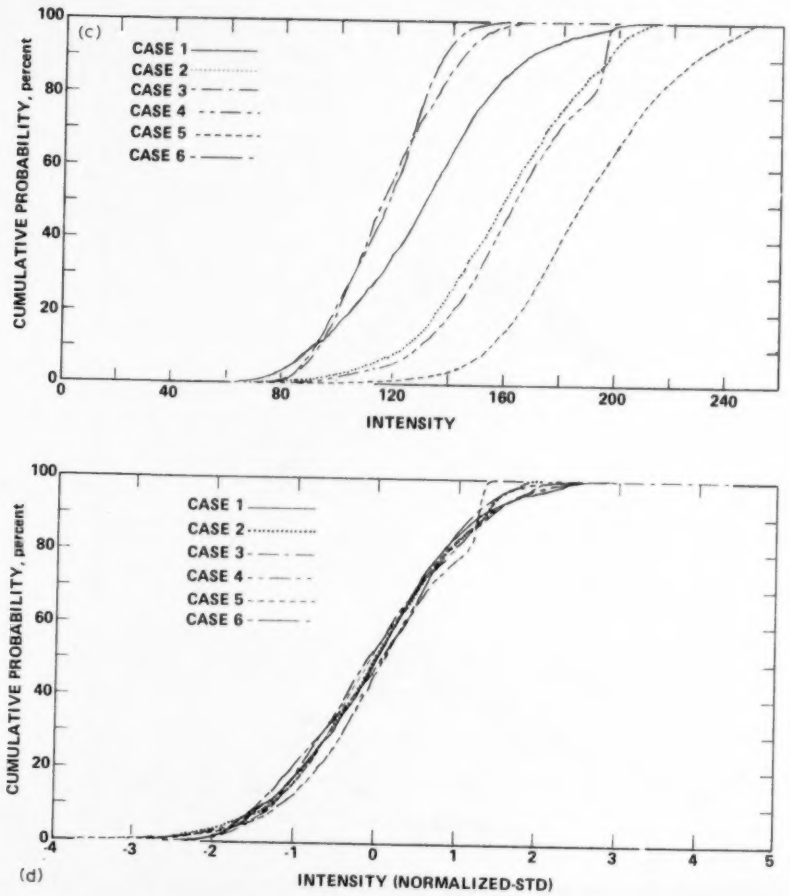

Fig. 7 (cont.). (c) Cumulative probability for original values; (d) cumulative probability for normalized values.

changes in the camera field of view, variation in the digitized position, or differences in the reflectivity of the surface. The smoke generator has no calibration and thus neither the volume of smoke source nor the particle size distribution could be precisely controlled. The situation was visually monitored during these experiments to ensure that there were no dramatic changes during the short time span for each case. There was probably no significant change during an individual case.

The coefficient of variation (CV = 100% × STD/MEAN) provides a good statistic for evaluating structurally similar pictures. The comparable values near the center of the flow field fell within 40°–60%, which is probably indic-

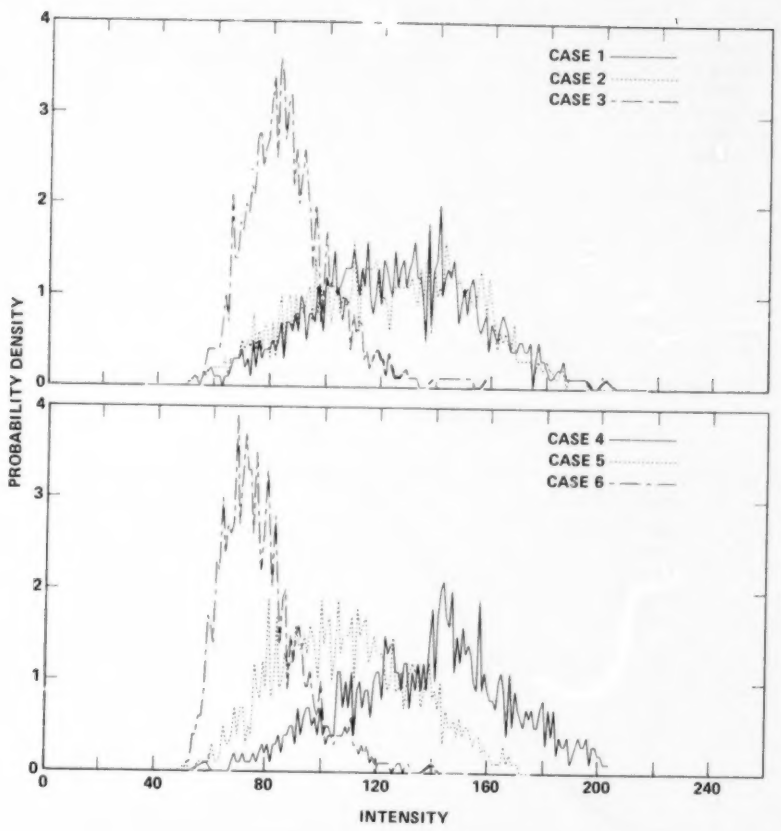

Fig. 8. Distributions for video image intensity series for side-view pixels at $x/H=3$, $z/H=0.5$: (a) probability density for original values.

ative of shedding vortices. The comparable values of CV are not affected by differences in velocity or building scale. The variation for the longitudinal velocity (see Table 2) was similarly 40–60%.

Figures 5 and 6 present plots of 15-s series using 30 samples per second. The fluctuating intensities about the series mean were normalized by their standard deviations as were done for velocity series. These time series provide a good indication of the potential usefulness of further analyses. The dominant period of fluctuation is proportional to the ratio of building height to mean velocity. The similar-looking behavior and the expected differences in the dominant periods of oscillation provide further support for the assumption

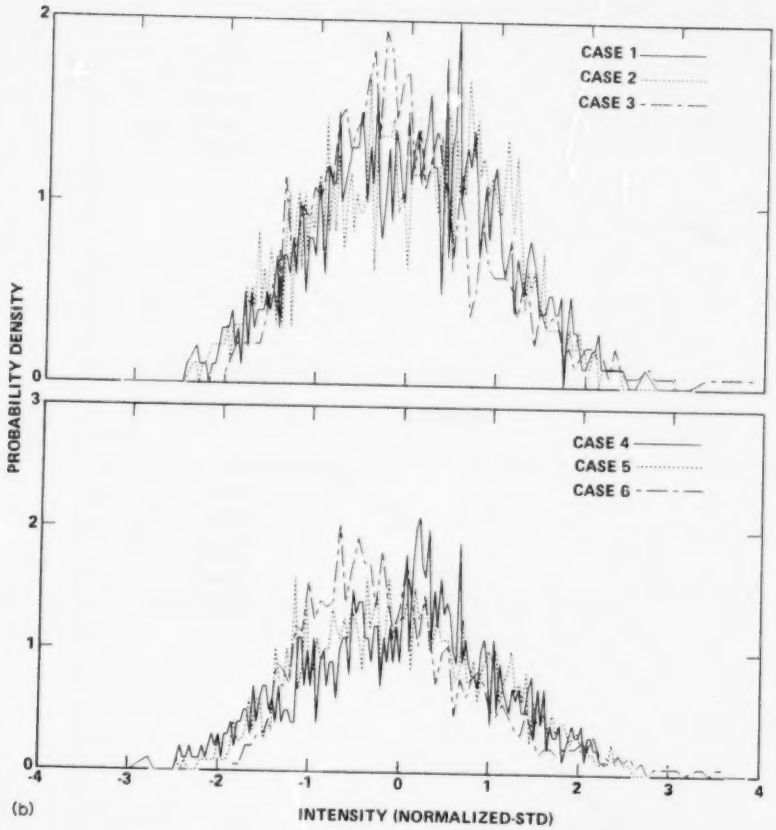

Fig. 8 (cont.). (b) Probability density for normalized values.

that the intensities of the recorded images meaningfully represent the periodic passage of the shed vortices.

Probability densities of the pixel intensity values for 45-s series using 60 samples per second (2700 values) are presented in Figs. 7 and 8. If the flow in the wake of the building is structurally similar for each case and the luminance is proportional to the smoke density, then the distributions of intensity (adjusted for background) should be the same. The probability densities for the normalized intensities are all quite comparable and so are the cumulative probabilities for the normalized values. The spike in case 4 (Fig. 7(b)) is believed to indicate that the digitized series was clipped for intensity above 200. The cause of the clipping is probably an instrument malfunction and is being further investigated. However, the data are valid for the purposes here. The clipped

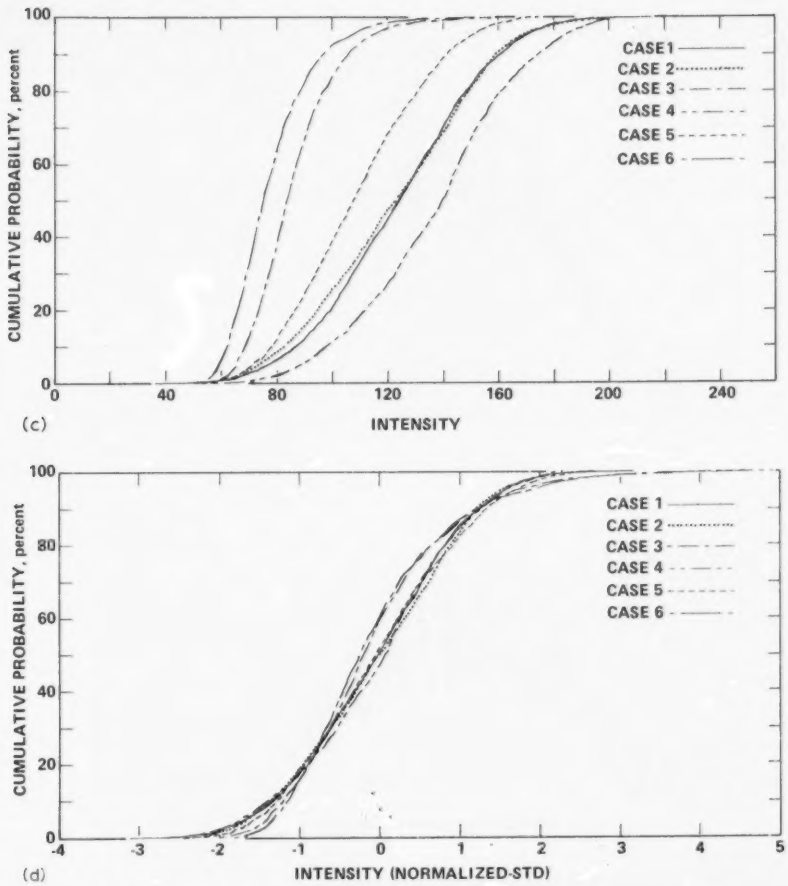

Fig. 8 (cont.). (c) Cumulative probability for original values. (d) cumulative probability for normalized values.

range appears to have a relatively insignificant effect on these analyses. Greater differences were found at $y/H=1$ and $z/H=1$, which were due to increased sensitivity in the outermost flow to the experimental precision. To find that normalized pixel intensities in the six cases, which cover a 16-fold range in average dilution, follow the same probability distribution is very supportive of the earlier assumptions made for these analyses. Effects of differences in background and processing noise among the six cases are not significant for series of intensities fluctuating about their mean. Thus, time series analyses of original fluctuating intensity do not require preprocessing. Keep in mind that each

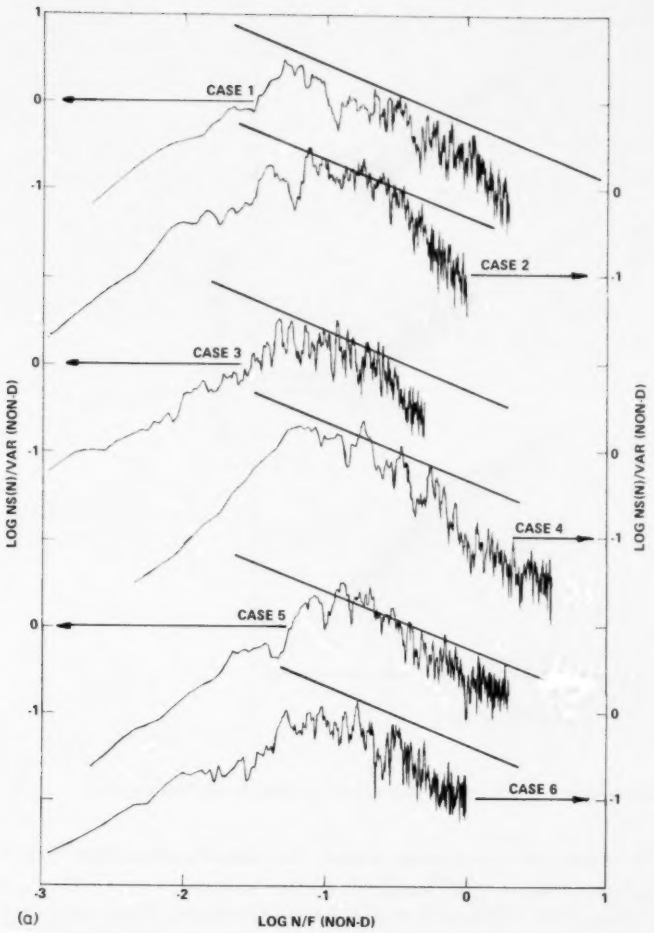

Fig. 9. Spectra for video image intensity series for top-view pixels: (a) all cases at $y/H=0$. The solid lines have a $-2/3$ slope.

smoke image represents a two-dimensional view of smoke-scattered light in the third dimension.

3.3.3. Time–space analysis

Spectra were calculated for 45-s series using 60 values per second. These were then normalized by the procedures given in Section 3.1 for the velocity spectra. The resulting spectra for cases 1–6 are shown in Figs. 9(a) and 10(a).

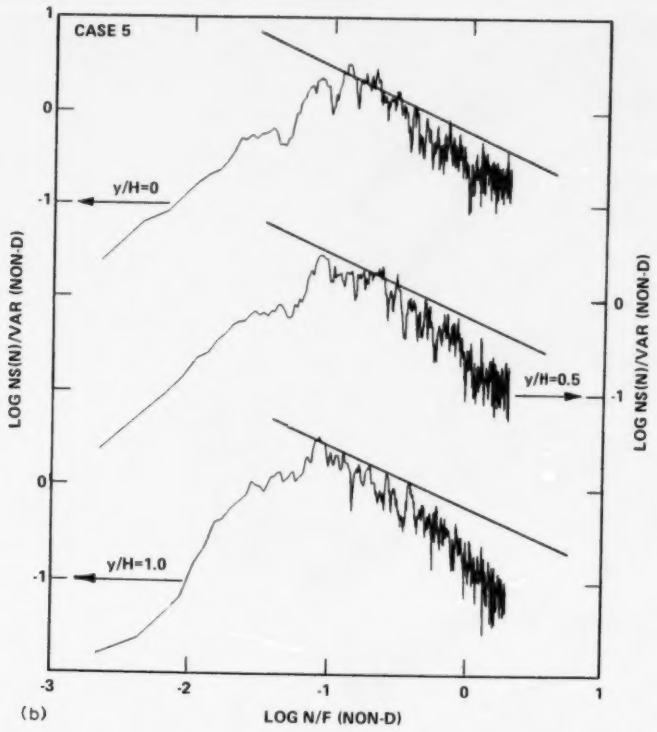

Fig. 9 (cont.). (b) Case 5 at $y/H=0$, 0.5, and 1. The solid lines have a $-2/3$ slope.

The variance for the series was used to normalize the spectral densities within each plot. The dominant frequencies for the top-view pixels at $y/H=0.5$ and $y/H=1$ for case 5 (Fig. 9(b)) fell within the 0.05–0.15 band. The dominant frequencies for the side-view pixels at $z/H=0.5$, 1, and 2 for the same case (Fig. 10(b)) fell within the 0.1–0.3 band. The apparent discrepancy between the two bands is explained by the difference between the top view and the side view of the shed vortices. Pixels from the top view measure passing smoke only when it moves downstream through its fixed lateral position, whereas the side view measures passing smoke at any cross-stream position. Since the vortex shedding tended to oscillate from side to side, it was expected that the dominant frequency for the side view would be twice that for the top view. The top-view pixels at $y/H=0$ should have been somewhat affected by each side of the flapping and were observed to have dominant frequencies comparable with the higher frequencies for the side-view pixels. The spectra for the side-view pixels at $z/H=0$ (Fig. 10(b)) have reduced dominant frequencies similar to those

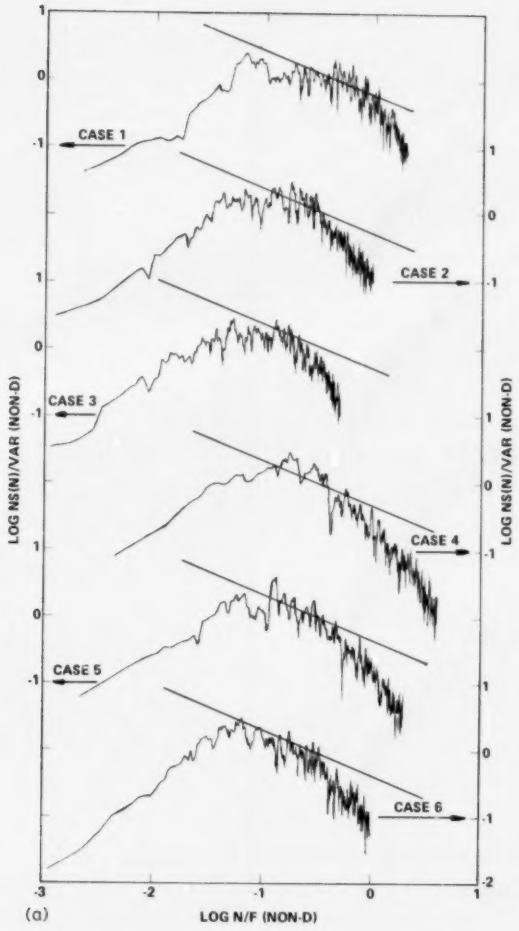

Fig. 10. Spectra for video image intensity series for side-view pixels: (a) all cases at $y/H=0$. The solid lines have a $-2/3$ slope.

for the top-view pixels. This was probably due to a smaller velocity below the roof-top. Thus, the overall depiction gained from these analyses is supportive of an arch-type vortex shedding from the building side and roof edges. Cross-stream integrated views (vertical pixel) near the roof level should contain all shed vortices, thus having a dominant frequency higher than away from the building roof edge or cross-stream from the building center. The midband of

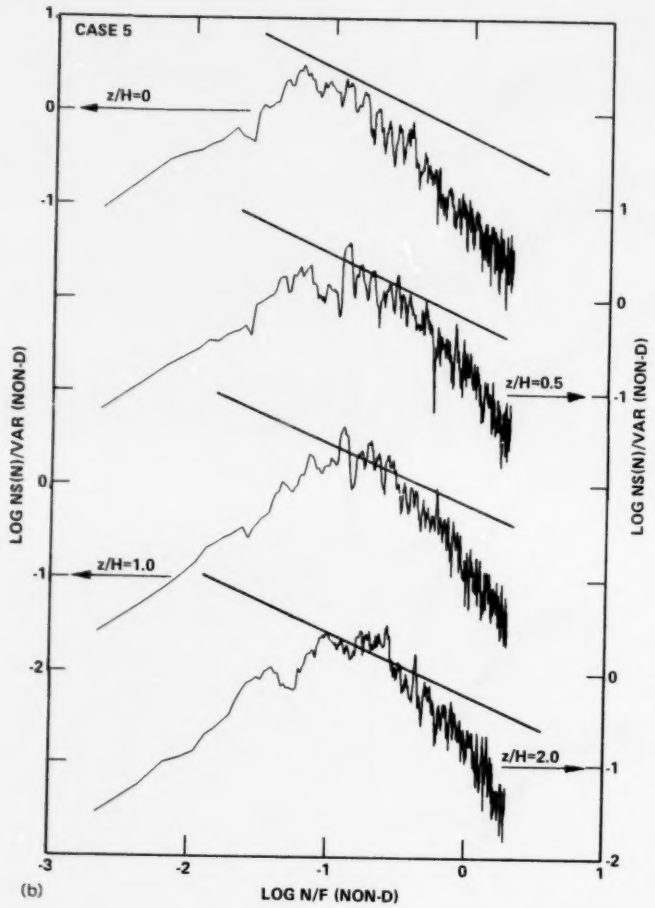

Fig. 10 (cont.). (b) Case 5 at $z/H=0$, 0.5, 1, and 2. The solid lines have a $-2/3$ slope.

highest dominant frequencies for these smoke images was 0.15, which was equal to that determined from the velocity spectra. The position of the velocity measurements was such that they should contain effects from all shed vortices.

A line with a slope equal to $-2/3$ is included on each of the spectrum plots. The spectra indicate that only a narrow band of frequencies just beyond the maximum may follow the theoretical inertial subrange estimate, as was observed for the velocity spectra. At higher frequencies, the spectral densities fall and their slopes are near -1 for the top-view pixels and near -2 for the side-view pixels. Estimates and observations of covariance spectra are shown by Kaimal et al. [10] to have slopes in the -1 to -2 range throughout an inertial

subrange. Pixel intensities represent the scattered light by smoke particles, integrated through the field of view, and should thus depend on the spatial covariance scale of smoke density through the field of view. Therefore, the largest pixel values result from large coherent patches of dense smoke. The largest patches should influence the spectral density at lower frequency more than at higher frequency. Small patches of locally dense smoke should be effectively smoothed by the integrated field of view. Steeper slopes throughout an inertial subrange should result for situations having a greater dependence on the spatial covariance scale. For these smoke studies, the spectral densities are distorted by the spatial averaging. The vertical pixel spectra are most distorted since they may represent a spatial integration over puffs originating at opposite sides of the building. This would in effect blur the smoke pictures and diminish higher frequency fluctuations.

Autocorrelations were also calculated for 45-s series using 60 values per second. The procedure was the same as that used for the velocity autocorrelations. The results are presented in Figs. 11 and 12(a). Figure 12(b) includes vertical pixels at $z/H=1.5$ and $z/H=2$ because a trend with height was noticed and further explored. Temporal integral scales and corresponding spatial scales using the nominal velocity (mean velocity without building) for each case were calculated as was done for the velocity series. Since the spectral peak corresponded to the dominant frequency of vortices being swept downstream, the spatial scale represents the characteristic size of these vortices. These vortices were carried at velocities close to those in the absence of the building.

From the top view (Fig. 11), the cross-stream pixel temporal scales for cases

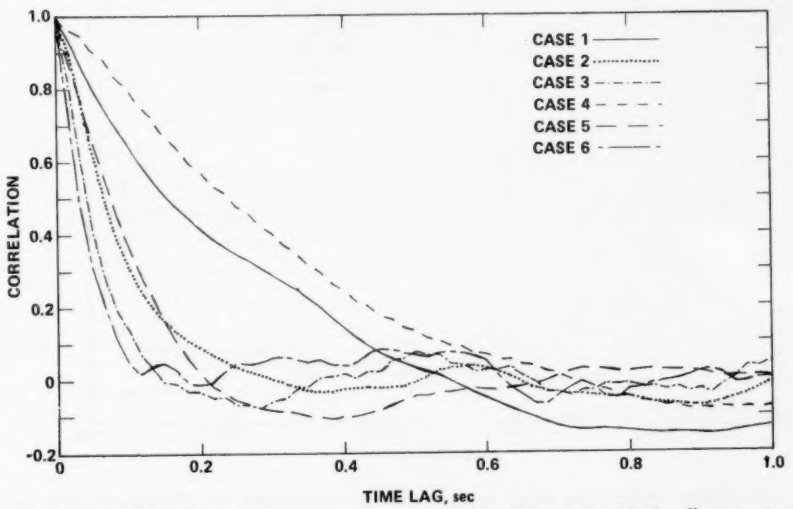

Fig. 11. Autocorrelation for video image intensity series for top-view pixels, all cases at $y/H=0$.

4–6 were not significantly larger than for cases 1–3. Differences among off-centerline pixels were somewhat larger. For both buildings, the temporal scales decreased with increasing velocity. However, the expected full effect of changing building scale was not observed. The characteristic sizes of vortices were 0.2 m and 0.3 m for the 0.1-m and 0.2-m buildings respectively. The size based on the velocity autocorrelation for the 0.2-m building was 0.2 m. The difference between the size for the smoke image and that for velocity may well be due to

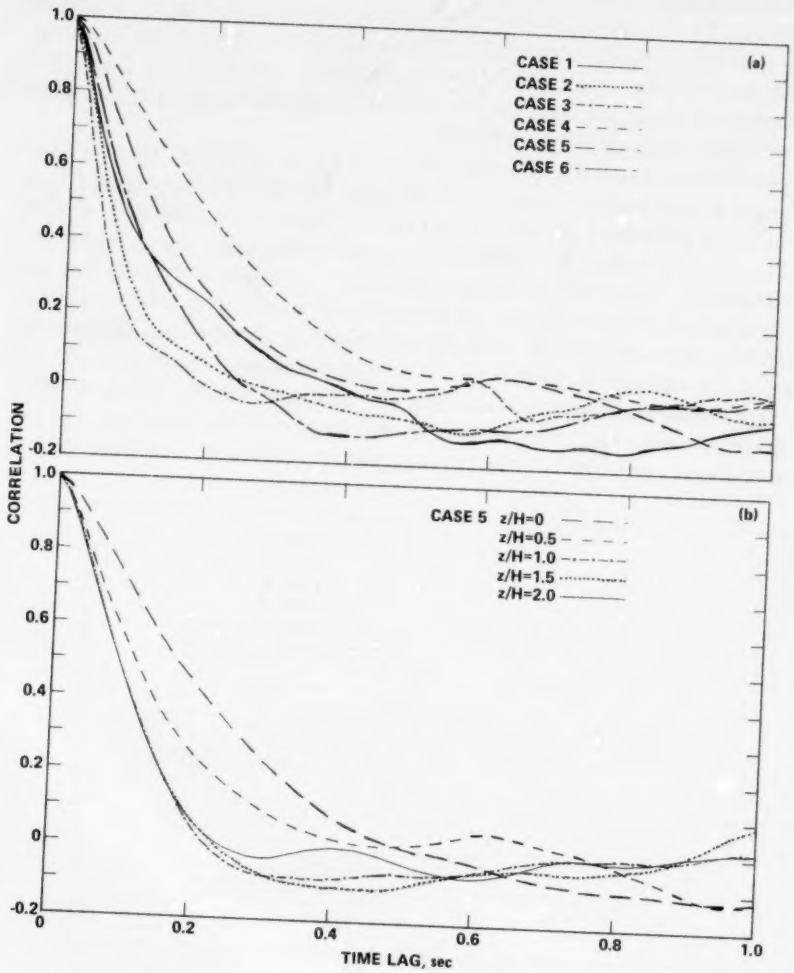

Fig. 12. Autocorrelation for video image intensity for side-view pixels: (a) all cases at $z/H=0.5$; (b) case 5 at $z/H=0$, 0.5, 1, 1.5, and 2.

the effects of wind shear. The top view of the smoke represents a vertically integrated profile. The effect of shear should be greater on the smaller building. The greater the velocity shear over the vortex, the greater will be its effect on enhancing the along-stream puff scale.

From the side view (Fig. 12(a), the vertical pixel time scales followed the appropriate trends. The full effect of changing building size was realized. However, only half the full effect of changing the velocity was realized. This could be explained by interference among cross-stream offset vortices as they passed through the side view. The interference should increase with increased velocity. Perhaps a look at some conditional statistics and analyses of a larger part of the picture will clarify the present observation. The effect of pixel elevation can be seen in Fig. 12(b), in which the change in the temporal scale followed the wind shear profiles. The characteristic lengths for case 1 ($H=0.1$ m) and case 4 ($H=0.2$ m) at $z/H=0.5$ were 0.1 m and 0.2 m respectively. These values are consistent with their expected values based on the velocity analyses. The deviation from expectations increased with increasing velocity, which supports the possibility that there may be blurring among puffs owing to significant spatial averaging, as discussed above.

4. Conclusions

The applicability of analyzing video pictures to study smoke dispersion was favorably demonstrated. The spectra and autocorrelations were comparable with those for velocity signals. An eightfold range in frequency scale and a 16-fold range in smoke dilution provided a good evaluation. Shedding vortices were clearly visible in the smoke pictures and quantifiable by the analyses. The dominant shedding frequencies near the center of the wake flow, normalized by the ratio of nominal velocity to building height, were found to be 0.1–0.3. The dominant shedding frequencies were lower away from the wake center because of increased intermittency. The visually observed and the broad band of dominant frequencies were indicative of arch-type vortices peeling off the building sides and roof. This is distinctly different from the classical von Karman vortex street. Estimated integral length scales near the center of the wake flow were found to be 1–2 times the building height. The recorded smoke images were two-dimensional pictures of integrated smoke particle density in the third dimension. Only data measured downstream at 3 times the building height were analyzed here. At a fixed downstream position, changes in the mean intensity of smoke-scattered light were found to follow changes in expected smoke particle density. However, comparisons between values at different downstream distances were affected by differences in illuminance and the light-scattering angle between the light beam and the camera amongst other things. Additional new analyses of segments of these pictures should clarify a few unresolved issues concerning the complex physics of the light-scattering pro-

cess. Alternative analyses of lighted sheets of smoke should perform as well, and would provide detailed nonintegrated point information, which would minimize the spatial distortion observed here.

Acknowledgements

I greatly appreciate the guidance and assistance on the use of the video sequence processor provided by Dr. Sarah Rajala and Mr. Adnan Alattar, Department of Electrical and Computer Engineering, North Carolina State University, through, in part, a Cooperative Agreement with the U.S. Environmental Protection Agency (CR807854 initially, and CR813368). The initial support provided under CR807854 was possible through the cooperation of Dr. S. Pal S. Arya, principal investigator. His encouragement and comments have been particularly helpful. I am also grateful to the staff of the U.S. Environmental Protection Agency Fluid Modeling Facility for assistance with the wind-tunnel experiments. The pulsed-wire anemometry was done in collaboration with Dr. William Snyder.

References

1 A.H. Huber and S.P.S. Arya, An investigation of transient aspects of atmospheric dispersion processes in the wake of a building through video image analysis, Proc. 7th Symp., on Turbulence and Diffusion, November 12–15, 1985, Boulder, CO, American Meteorological Society, Boston, MA, pp. 18–21.

2 A.H. Huber and W.H. Snyder, Wind tunnel investigation of the effects of a rectangular-shaped building on dispersion of effluents from short adjacent stacks, Atmos. Environ., 16 (1982) 2837–2848.

3 A.H. Huber, Evaluation of a method for estimating pollution concentrations downwind of influencing buildings, Atmos. Environ., 18 (1984) 2313–2338.

4 J.H. Vincent, Model experiments on the nature of air pollution transport near buildings, Atmos. Environ., 11 (1977) 765–774.

5 A.S.M. MacLennan and J.H. Vincent, Transport in the near aerodynamic-wakes of flat plates, J. Fluid Mech., 120 (1982) 185–197.

6 J.C.R. Hunt, C.R. Abell, J.A. Peterka and H. Woo, Kinematical studies of the flows around free or surface-mounted obstacle; applying topology to flow visualization, J. Fluid Mech., 86 (1978) 179–200.

7 I.P. Castro, Measurements in shear layers separating from surface-mounted bluff bodies, J. Wind Eng. Ind. Aerodyn., 7 (1981) 253–272.

8 H. Sakamoto and M. Arie, Vortex shedding from a rectangular prism and a circular cylinder placed vertically in a turbulent boundary layer, J. Fluid Mech., 126 (1983) 147–165.

9 SAS Institute Inc., SAS®/ETS User's Guide Version 5 Edition, Cary, NC: SAS Institute Inc., 1984, 738 pp.

10 J. Kaimal, J. Wyngaard, Y. Izumi and O. Cote, Spectral characteristics of surface-layer turbulence, Quart. J.R. Met. Soc., 98 (1972) 563–589.

11 I.P. Castro and A. Haque, The structure of a turbulent shear layer bounding a separation region, J. Fluid Mech., 179 (1987) 439–468.
12 F. Pasquill, Atmospheric Diffusion, Ellis Horwood, Sussex, England, 1974, p. 130.
13 N.A. Fuks, The Mechanics of Aerosols, Pergamon, Oxford, English edn. 1964, pp. 7–30.
14 R.E. Rosensweig, H.C. Hottel and G.C. Williams, Smoke-scattered light measurement of turbulent concentration fluctuations, Chem. Eng. Sci., 15 (1961) 111–129.
15 H.A. Becker, H.C. Hottel and G.C. Williams, On the light-scatter technique for the study of turbulence and mixing, J. Fluid Mech., 30 (1967) 259–284.
16 E.J. Shaughnessy and J.B. Morton, Laser light-scattering measurements of particle concentration in a turbulent jet, J. Fluid Mech., 80 (1977) 129–148.
17 M.B. Long, B.T. Chu and R.K. Chang, Instantaneous two-dimensional gas concentration measurements by light scattering, AIAA J., 9 (1981) 1151–1157.
18 B. Yip, Y.K. Lam, M. Winter and M.B. Long, Time-resolved three-dimensional concentration measurements in a gas jet, Science, 235 (1987) 1209–1211.
19 R.T. Yang and R.N. Meroney, A portable laser light-scattering probe for turbulent diffusion studies, Rev. Sci. Instrum., 45 (1974) 210–215.
20 H.C. van de Hulst, Light Scattering by Small Particles, Wiley, New York, 1957, pp. 1–57.

Appendix: Apparatus

A.1. The wind-tunnel facility and associated instrumentation

The experimental study was conducted in the U.S. Environmental Protection Agency's Meteorological Wind Tunnel. It is an open-return wind tunnel with a test section 2.1 m high, 3.7 m wide, and 18.3 m long. The tunnel controller can provide steady free-stream speeds of 0.3–8 m s^{-1}. In the present experiments free-stream speeds ranged from 1–5 m s^{-1}. A 15.5 cm fence was placed 22.3 cm downstream of the beginning of the test section to develop a thick boundary layer. The tunnel floor was covered with gravel (<10 mm diameter) to provide an appropriately rough surface. The building was placed at 8 m downstream of the beginning of the test section. By this distance, the depth of the growing boundary layer has stabilized at near 1 m. Previous comparable studies have shown that in the absence of building effects tracer plume dispersion behaves like that in a neutrally stable atmospheric flow. Further details of the wind tunnel and its operating characteristics are given by Snyder [A1]. Guidance and standard operating procedures that were followed are described by Lawson [A2]. See Bradbury and Castro [A3] for a discussion on the pulsed-wire measurement technique. Those reports include detailed discussions on the instrumentation briefly discussed here.

Velocity and turbulence data were obtained with constant-temperature anemometers in conjunction with x-array hot-wire probes (end flow style) and with a pulsed-wire anemometer. Calibrations were performed in the free stream using reference to pitot-static measurements. The reported sampling rates for the hot-wire probes of up to 500 per second were well within normal response for the hot-wire instrumentation. The 60 samples per second rate for the pulsed-wire probe was near its upper limit. It was not possible to collect a series of samples without including some values resulting from premature triggering.

These seem to result both from thermal fluctuations drawn through the wind tunnel and the late arrival of probe heat pulses. A more detailed evaluation of these problems is needed. Here, the false samples were recalculated as the average over the interval before and after. These difficult samples accounted for less than 0.3% of the samples for the case 5 components. The higher speed case 6 had almost no bad samples.

The hydrocarbon tracer measurements used ethane as the source. Concentrations were measured with a flame ionization detector that was operated continuously over the sampling period. The response characteristics for the detectors are such that only mean values over sufficient time are available. Averaging periods of 1–2 min have been found sufficient in previous studies; therefore, the measurements reported here are for 1.5–2 minute averages. The hydrocarbon samples were drawn from a rake of tubes positioned in the wind-tunnel flow. A background concentration sample was taken prior to and after the end of a series of plume concentration measurements. The background concentration was assumed to change linearly over time. The estimated background was then subtracted from each of the measurements. Background concentrations were less than 1% of the plume centerline concentrations. The adjusted concentrations for even the lower values near the tails of the plume were precise, provided the background changed linearly over the time average. Problems with the changing background were avoided by constantly monitoring the background concentration. The ethane tracer source rate was calibrated and maintained constant during each measurement.

The building Reynolds number based on the building height H as a length scale and the mean velocity at $0.5H$ as a velocity scale ranged from 6000 for case 1 to 50 000 for case 6. Only case 1 fails to exceed the generally accepted value of about 11 000 for the Reynolds number to obtain Reynolds-number-independent flow over block-shaped buildings (Snyder [A4]). It is believed that the measurements for case 1 were reliable for the purposes here. However, the results for case 1 should be considered cautiously.

A.2. Image recording and analysis instrumentation

An RCA model TC1005 black-and-white camera having a low-bloom silicon vidicon target (1 inch) was used. The camera gamma correction is internally variable and was factory set to 1 for providing linearity between the light intensity on the target and the voltage output. The camera was connected to a JVC model HR-2200U VHS format video cassette recorder. A check on the camera and recorder response is reported below.

The NTSC composite signal system is used. The system format includes 525 lines that are interlaced at 1/60 s out of phase. There are 30 pictures per second. A video sequence processor (VSP) was used for analog-to-digital conversion of the video luminance signal. The VSP is part of the Image Processing Laboratory in the Department of Computer and Electrical Engineering at North

Caroline State University. The recorded camera field of view is digitized at a resolution of 525 lines (vertical) by 768 picture elements per line (horizontal). Actual digitization was limited to a small window of interest (i.e. several lines by several hundred picture elements). The luminance signal was digitized on an integer scale of 0–255 (8 bits). The recorded field of view was approximately 1.5 m by 1 m. Each evaluated picture element was found to correspond to a 2.2-mm-square field of view.

Figure A1 presents a check on the response of the camera and the recorder. Their response to changing illumination from light reflected from a standard gray scale card was read from a waveform monitor set up for NTSC signal analyses. The camera response for three different levels of uniform background illumination was evaluated. The tape-recorded signal for level 1 was also evaluated in comparison with the straight camera response. Relative illumination levels of 1, 2.12, 4, 8.16, 16 and 32.85 correspond to the relative illumination on the camera target for the camera *f*-stops of 16, 11, 8, 5.6, 4, and 2.8 respectively. The response intensity is scaled so that 0–100 corresponds to the standard full range of luminance. The response with the lens capped was found to be 17. This level is above the standard reference black level of 7.5. The response was observed to be linear within the standard range between 0 and 100. The response above 100 indicates the effects of electronic clipping which are built into the camera and recorder to prevent damage from voltage

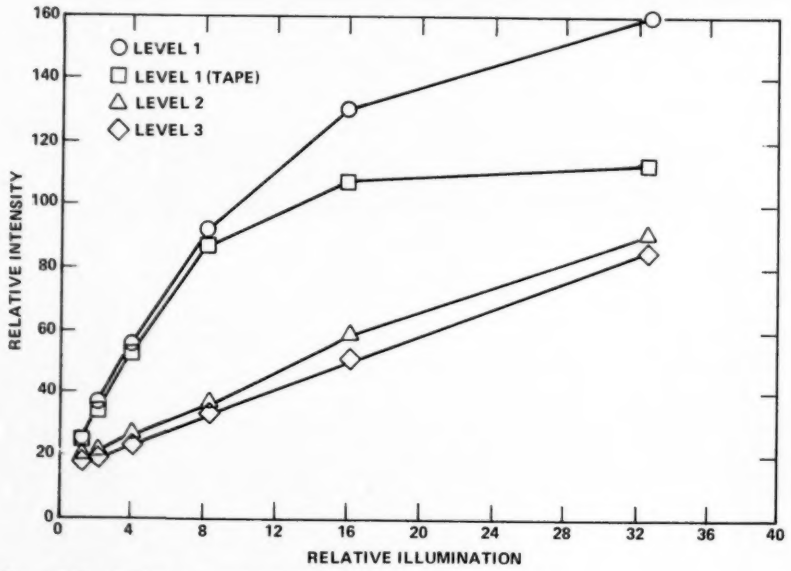

Fig. A1. Evaluation of camera response.

overdrive. The tape-recorded signal was more strongly clipped. These results are very relevant to understanding the digitized video values. The digitizer was designed to be linearly scaled from 0 to 255 (8 bit resolution) over the standard range of 7.5 to 100 respectively. The observed highest digitized value of 255 should correspond to the standard 100 (or a saturated value above 100) level. An observed lowest digitized value of 26 should correspond to the capped level of 17 which is 10% of the standard black level of 7.5. The digitizer was designed with the added protection of a guard band which locks on the signal at levels corresponding to digitized values between 16 and 240. The guard band has been observed to be shifted relative to the standard range, resulting in digitized values that have an added constant value.

References to Appendix

A1 W.H. Snyder, The EPA meteorological wind tunnel: its design, construction, and operating characteristics, U.S. Environmental Protection Agency Rep. No. EPA-600/4-79-051, Research Triangle Park, NC, 1979.

A2 R.E. Lawson, Jr., Standard operating procedures for the EPA Fluid Modeling Facility, U.S. Environmental Protection Agency, FMF Internal Document, Research Triangle Park, NC, 1984.

A3 L.J.S. Bradbury and I.P. Castro, A pulsed-wire technique for velocity measurements in highly turbulent flows, J. Fluid Mech., 49 (1971) 657-691.

A4 W.H. Snyder, Guideline for fluid modeling of atmospheric diffusion, U.S. Environmental Protection Agency Rep. No. EPA-600/8-81-009, Research Triangle Park, NC, 1981.

NOTICE

This document has been reviewed in accordance with U.S. Environmental Protection Agency policy and approved for publication. Mention of trade names or commercial products does not constitute endorsement or recommendation for use.

This article documents research that was conducted under the auspices of the U.S. Environmental Protection Agency (USEPA). As an arm of the government, the USEPA has a paid up, non-exclusive, irrevocable, worldwide license to reproduce, prepare derivative works, and distribute to the public all of the material contained herein, and to grant others acting on its behalf the right to do so. The USEPA grants to the National Technical Information Service, Department of Commerce, the right to act as its agent in the distribution of this material.